Hindawi
Journal of Chemistry
Volume 2019, Article ID 7472058, 12 pages
https://doi.org/10.1155/2019/7472058

Research Article

Halloysite Nanotube-Reinforced Ion-Incorporated Hydroxyapatite-Chitosan Composite Coating on Ti-6Al-4 V Alloy for Implant Application

Manickam Chozhanathmisra,[1] Kannaiyan Pandian,[2] Dharman Govindaraj,[3] Palanisamy Karthikeyan,[4] Liviu Mitu,[5] and Rangappan Rajavel[1]

[1]*Department of Chemistry, Periyar University, Salem 636011, Tamilnadu, India*
[2]*Department of Inorganic Chemistry, University of Madras, Guindy Campus, Chennai 600025, Tamilnadu, India*
[3]*Department of Natural Products Chemistry, School of Chemistry, Madurai Kamaraj University, Madurai 625021, India*
[4]*Department of Chemistry, Periyar University Constituent College of Arts and Science Idappadi, Salem 637102, Tamilnadu, India*
[5]*Department of Physics & Chemistry, University of Pitesti, Pitesti 110040, Romania*

Correspondence should be addressed to Liviu Mitu; ktm7ro@yahoo.com and Rangappan Rajavel; drrajavelpu@gmail.com

Received 22 October 2018; Revised 29 December 2018; Accepted 3 January 2019; Published 6 March 2019

Academic Editor: Jean-Marie Nedelec

To develop the corrosion resistance and improve the biological performance of a titanium implant (Ti6Al4V alloy), a series of mineral (M = Zn and Mg)-substituted hydroxyapatite (MHA), chitosan-MHA (CS-MHA), halloysite nanotube-MHA (HNT-MHA), and HNT-CS-MHA composite coatings were fabricated on the anodized titanium alloy by electrodeposition. The surface morphology and cross section of various coated composites were investigated by high-resolution scanning electron microscopy (HR-SEM). Furthermore, the functional groups and phase structure of the composite coatings were investigated by Fourier transform infrared spectroscopy (FTIR) and X-ray diffractometry (XRD). Corrosion behaviors of the composite coatings were also investigated by polarization and impedance spectroscopy (EIS). Moreover, the cell-material interaction of the composite coating was observed *in vitro* with human osteoblast MG63 cells for cell proliferation at 1, 4, and 7 days of incubation. Consequently, HNT-CS-MHA-Ti may have potential applications in the field of orthopedic and dental implants.

1. Introduction

Biomaterials are natural or artificial materials currently used in making implants or structures, which should be chemically and biologically active to the surrounding tissues and human body fluid [1]. Biologically active implants increase their quality of life and longevity of human beings. In this case, metal-based biomaterials are used for long time load-bearing implant prostheses for several years [2]. Especially, Ti and its alloys are used in biomedical devices for internal fixation devices (such as pins, screws, bone plates, and others), among which orthopedic implant applications are relatively effective due to their low density, high strength, appropriate biocompatibility, and excellent corrosion resistance [3]. However, the surface of Ti alloy loses its efficiencies because the human body fluids leach out aluminum and vanadium ions; because of their inefficiency to form a chemical bond with bony tissue, loosening may occur over a long period, becoming a critical problem known as poor osteoconductivity; furthermore, a high concentration of these metal ions causes a negative effect on living organisms [4].

In this circumstance, implant surfaces cannot chemically bond with natural bones, and also they do not support new bone formation. Failures of Ti alloys as metallic implant surfaces have also been reported widely and mainly due to corrosion and fatigue [5]. Anodic oxidation has become an attractive method for preparing oxide films on titanium alloy

surfaces because the oxide films prepared in this way exhibit porous microstructure with rounded pores and ensure apatite formation in the physiological environment in order to improve implant bioactivity for biomedical applications. Thus, the corrosion-resistant, bioactive, and surface modifications of the medical implant surfaces are required [6].

Many methods have been developed to improve the bioactive and corrosion-resistant coating of polymer composites or bioceramic coating materials like hydroxyapatite (HA). Calcium hydroxyapatite, Ca_{10} $(PO_4)_6(OH)_2$, is the inorganic constituent of synthetic biomaterials, is present in 70% weight of human bones and hard tissues, and is widely applied to bone repair for replacements and bone substitute material [7]. It has been recently reported that HA can be used as a coating material for implant surfaces and also possesses excellent bioactivity and longer osteoconductivity [8]. The HA forms chemical bonding between biomedical implants' surfaces and natural bones, makes its coating to stimulate new bone formation, and improves human bone tissue osseointegration because its structural, chemical, crystallographic, and mineralogical compositions are similar to bone minerals [9].

HA has a suitable material for coating on Ti6Al4V alloys to improve the bioactivity and decrease the degradation rate [10]. However, pure HA cannot be used for a long-time high-load-bearing implant prosthesis because of its poor biological activity such as low antibacterial activity and poor mechanical properties such as material brittleness, bending strength, and low fracture toughness; furthermore, biological materials with some metallic antibacterial agent-substituted HA coatings to improve the biological properties of the implants show antimicrobial activity [11, 12].

It is recently reported that mineral-substituted HA possesses excellent biological properties. Enhanced antimicrobial property, long-term biostability, and cell-material interactions could be obtained for MHA-coated metallic implant surfaces [13]. Among other divalent cationic substitutions for Ca in the HA lattice, a homogeneous Zn-HA coating on implant surfaces prepared by the electrodeposition method showed good apatite formation ability [14]. Therefore, it is desirable that mineral-substituted HA coatings be applied on the Ti alloy for biomedical applications [15]. Magnesium (Mg) is one of the most abundant divalent cations in the human body. Mg plays an important role in promoting cellular adhesion onto the substrate [16], enhancing osteoblast cell activity, bone development, and inhibiting osteoclasts [17].

Chitosan (CS) is a naturally occurring cationic polysaccharide containing hydroxyl groups and amino groups and is a very useful polymer for tissue engineering due to its antibacterial property, biocompatibility, bioactivity, hydrophilicity, and nontoxicity [18]. CS can be used as a film-forming agent, charging agent, and dispersing agent and allows for deposition of composites, containing the CS matrix of hydroxyapatite (HA) and HNT. CS has been briefly active in improving new bone formation. CS can be utilized in combination with biologically active polymers and ceramics to further enhance tissue-regenerative efficacy [19]. However, an easy agglomeration or gel formation, the mechanical properties, low specific gravity, and thermal stability of CS could be improved by a different modification. Incorporation of nanosized inorganic materials such as titanium dioxide, carbon nanotubes, hydroxyapatite, graphene, and nanoclay into CS can improve the mechanical properties of composites [20].

There is an increasing interest in the unique medical and biological properties of halloysite nanotubes (HNTs), and it is expected that biomaterials incorporating HNT will be developed for clinical uses. HNTs may be considered as a naturally available two-layered 3-dimensional aluminosilicate mineral clay ($Al_2Si_2O_5(OH)_4{\cdot}2H_2O$) [19]. In the past few years, HNTs have generated substantial interest in various types of organic/inorganic composites in biomedical applications [20]. Because of their large surface area, high porosity, strong stability, and tunable surface chemistry, they have attracted great interest in material science, especially drug delivery, catalysis, and anticorrosion coating, as compared to other nanomaterials, such as carbon nanotubes. HNTs are nontoxic for human and animal cells, particularly preventing the release of toxic elements in the implant surfaces. Recently, HNTs are used as a new type of filler for polymers to improve the mechanical and corrosion properties of the titanium implants [18–26]. Therefore, several coating techniques have been reported to fabricate HA composite coating on titanium-based alloy surfaces. Electrochemical deposition technique has numerous advantages compared with other coating techniques, due to low processing cost, less time consumption to grow uniform coatings, easy control of the thickness resulting in homogeneous morphology, and adjustment of the deposition time and applied potential [11, 12].

An attempt is made in the present work to get improved biological performance and better corrosion protection of the composite coating. This HNT-CS-MHA composite coating on the anodized Ti alloy is expected to be an alternative material for biomedical implants with enhanced biological and mechanical functionalities.

2. Materials and Methods

2.1. Materials. Halloysite nanoclay, chitosan (Mw = 200,000) with a deacetylation degree of 85%, commercially available pure calcium nitrate tetrahydrate ($Ca(NO_3)_2{\cdot}4H_2O$), zinc nitrate tetrahydrate ($Zn(NO_3){\cdot}6H_2O$), diammonium hydrogen phosphate ($(NH_4)_2HPO_4$), ethanol ((EtOH) (C_2H_5OH)), ammonium hydroxide (NH_4OH), acetic acid, and phosphoric acid (H_3PO_4) solutions were used in this study. All other chemicals used were of analytical grade and used as purchased from Sigma-Aldrich Chemical Co. (Aldrich, India). All the solutions were made up with deionized water. Electrodeposition of the composite coatings and the experiments were performed at room temperature.

2.2. Preparation of Ti Alloy. Commercially available Ti alloy (sheet) was used as an implant substrate material for coating the composites of hydroxyapatite; the implant substrates were cut into $10 \times 10 \times 3$ mm diameter, and the thickness of the implant substrate surfaces was ground with silicon

carbide (SiC) papers progressively to 120–2000 grit sizes and soaked with double-distilled water (DI). Furthermore, the implant substrates were ultrasonically cleaned with acetone for 30 min to remove oil and remaining grease and finally dried in air. The electrodes were cleaned in acetone/ethanol/water as solvents and used as a working electrode in the electrolytic solution for further electrochemical studies.

2.3. Preparation of Electrolyte. The electrolyte MHA was prepared by mixing solutions of 0.4 M $Ca(NO_3)_2{\cdot}4H_2O$, 0.05 M $Zn(NO_3){\cdot}6H_2O$, 0.05 M $Mg(NO_3){\cdot}6H_2O$, and 0.3 M $(NH_4)_2HPO_4$ in 1.67 ratio (Ca + Zn + Mg)/P; the prepared solution was continuously stirred, and the pH of the electrolyte solution was adjusted to 4.5 by adding a diluted solution of 0.1 M NH_4OH [12–14]. The MHA electrolyte was then deaerated for 15 min in N_2 atmosphere in order to reduce the amount of dissolved carbon dioxide and thus to minimize the formation of calcium carbonate deposits.

Chitosan was protonated by dissolving it in an acetic acid solution. Dilute CS solution was prepared by dissolving 2 g in 100 ml of 2% acetic acid solution and mechanically stirring at 250 rpm for 24 h at room temperature. The HNTs were prepared from a suspension of 0.1 g HNT in 100 mL of double-distilled water, and HNTs/distilled water solution was continuously stirred overnight followed by ultrasonication for 30 min at ambient temperature to achieve a homogeneous dispersion of HNTs [18, 19].

Electrochemical deposition was carried out in the electrolyte solution which was prepared by mixing the solutions of 10 mL of CS, 5 mL of HA, and 5 mL of HNT. Prior to electrodeposition, the electrolyte was stirred for 60 min and then sonicated for 30 min at ambient temperature to achieve a homogeneous distribution. No additive was added as a charging and/or dispersion agent.

2.4. Electrodeposition of Composite on Ti6Al4V. The electrodeposition of MHA, CS-MHA, HNT-MHA, and HNT-CS-MHA coatings on anodized Ti alloy implant surfaces from aqueous HNT, acetic acid solution of CS, and MHA was performed in the three conventional electrode cell configurations by the galvanostatic method using electrochemical workstation (CHI 760 C) in which the implant substrate was used as the working electrode and saturated calomel electrode (SCE) and platinum electrode as the reference electrode and counter electrode, respectively. All the potential values in the text are reported with respect to the SCE [22, 26].

2.5. Surface Characterization. The characteristic functional groups of composite-coated Ti alloy specimens were analyzed using FT-IR (Bruker Tensor-25) spectroscopy using KBr pellets. All the spectrums were recorded over the frequency range from 400 to 4000 cm^{-1} and spectral resolution of 4 cm^{-1} averaging over 32 scans. The crystal phase of composite-coated specimens was analyzed by X-ray diffraction (Rigaku Miniflex-II model) with monochromatic Cu Kα (target) radiation (wavelength of 1.5406 Å) at a voltage of 40 kV and a current of 30 mA. XRD patterns were collected for scanning range of 2θ values between 20° and 60° in a continuous mode at a scan rate of 10 min^{-1} and increment step size of 0.02° (2θ). Both FT-IR and XRD measurements were carried out using powders scraped from the deposited Ti alloy surfaces.

The surface morphology and elemental composition of the composite coated on Ti alloy samples were examined using high-resolution scanning electron microscopy (HR-SEM, JSM 840A Scanning Microscope, JEOL, Japan) equipped with energy dispersive X-ray spectroscopy (EDX).

2.6. Electrochemical Investigation. The electrochemical investigation of MHA-, CS-MHA-, HNT-MHA-, and HNT-CS-MHA-coated and uncoated Ti alloy samples were performed by potentiodynamic polarization (PD), and electrochemical impedance spectroscopy (EIS) was conducted in simulated body fluid (SBF) solution used as an electrolyte at a temperature of 37°C. SBF solution was prepared by dissolving the reagent-grade salts similar to the human blood plasma (Table 1), using the procedure proposed by Kokubo [27]. Electrochemical tests were carried out by the galvanostatic method using a conventional three-electrode cell system (electrochemical workstation CHI 760C USA). A three-electrode cell was set up with a working electrode (the coated and uncoated samples with the exposed area of 1 cm^2), a platinum counter electrode, and a saturated calomel electrode (SCE) as a reference electrode. The working electrode was kept in contact with the SBF solution to obtain a stable open circuit potential (OCP) for 60 min before the test. The polarization tests were conducted at the scan rate of 1 mVs^{-1} in the scan range of –0.8 to +0.2 V with reference to OCP. The electrochemical impedance spectroscopy (EIS) data were recorded at a frequency range from 100 kHz to 1 MHz with a signal amplitude of 5 mV [20, 24].

2.7. Antibacterial Assessment of Composite. The antimicrobial activities of the composite-coated scraped sample were investigated by Gram-positive (*Staphylococcus aureus* (ATCC 25923)) and Gram-negative (*Escherichia coli* (ATCC 25923)) bacteria through the agar well diffusion method. The bacterial stock solution was prepared by overnight broth cultures of *S. aureus* and *E. coli* tryptic soy broth with 0.6% yeast extract at room temperature with constant stirring. A culture suspension of the tested two strains was spread on a Mueller–Hinton agar media, and then, the prepared composite-coated samples were placed on the seeded agar plates followed by incubation for 24 h at 37°C. The diameters of the clear area indicating the zone of inhibition in the agar plate were measured and captured using an ordinary camera.

2.8. Evaluation of the Osteoblast Cell Viability. The *in vitro* cytotoxicity of the as-coated composite to human osteoblast MG63 cells (purchased from National Centre for Cell Science (NCCS), Pune, India (MG63, ATCC CRL-1427 TM)) was evaluated by MTT assay. The cytotoxicity tests were determined by indirect method, where the test cells (MG63)

Table 1: Ionic composition of human blood plasma and SBF (27).

Ion	Na^+	K^+	$Ca2^+$	$Mg2^+$	Cl^-	HCO_3^-	HPO_4^{2-}	$SO4^{2-}$
Human blood plasma (mM)	142	5	2.5	1.5	103.0	27.0	1.0	0.5
SBF (mM)	142	5	2.5	1.5	147.8	4.2	1.0	0.5

were cultured in Dulbecco's Modified Eagle Medium (DMEM, GIBCO), which consisted of a minimal essential medium (Hi Media Laboratories), supplemented with 10% fetal bovine serum (FBS, Biowest, France). The cultured MG63 cells were then incubated in the humidified atmosphere of 5% CO_2 and 95% air for 1, 4, and 7 days at 37°C. The tested sample of the HNT-CS-MHA composite coating under determination was sterilized in an autoclave at 140°C during 2 h and then was placed in well tissue culture plates in a humidified 5% CO_2 atmosphere. The MG63 cell culture media in each well of the tissue culture plate was renewed every 2 days, and the cultures were maintained in a humidified atmosphere of 95% air and 5% CO_2, at 37°C. The tested solution was then removed and added with dimethyl sulfoxide, and the plate was shaken for 10 min. Finally, the absorbance was recorded at 570 nm using a microplate reader to examine the viability of the HNT-CS-MHA composite sample, and the viability (%) was calculated in comparison with respect to the control as follows:

$$\%\ \text{cell viability} = \frac{[A]\text{test}}{[A]\text{control}} \times 100. \quad (1)$$

3. Results and Discussion

3.1. Surface and Elemental Analysis. HR-SEM observations of MHA, CS-MHA, HNT-MHA, and HNT-CS-MHA composite-coated Ti alloy specimens, respectively, are shown in Figures 1(a)–1(d). The surface morphology of the MHA-deposited coating on the Ti alloy specimen (Figure 1(a)) exhibited the formation of nonuniformly arranged spherical-like microstructure which appears to be loosely bound to the specimen substrate. The HR-SEM image of CS-MHA coating on implant specimen surface is entirely covered with sponge-like structure morphology (Figure 1(b)). Figure 1(c) shows the homogeneous distribution of rod with spherical-like microstructures observed for HNT-MHA. The HR-SEM image of HNT-CS-MHA composite-coated specimen surfaces from three components is shown in Figure 1(d). As can be seen, the surface of CS is mostly covered by HA and HNT. As shown in Figure 1(e), the cross section of HNT-CS-MHA composite coating demonstrated a 50 μm thick coating, which was dense, uniform, and crack-free. There is an adhesion between the deposited coating and the implant surface (Figure 1(e). This indicates that the HNT-CS-MHA coating can tightly adhere to the implant substrate. Hence, the deposited implant surfaces may provide more corrosion protection in stimulated body fluid environment [28, 29]. Figure 1(f) shows the elemental mapping of HNT-CS-MHA composite coating, which indicates the presence of Ca, P, Al, Si, O, Zn, Mg, C, and N ions in the HNT-CS-MHA coating. The uniform distribution of metal ions was well-evidenced by the elemental mapping results. Hence, this composite coating is thought to be favorable for cellular processes due to the presence of minerals such as Zn, Mg, and CS in HA.

3.2. FT-IR Analysis. The functional group analysis of the MHA, CS-MHA, HNT-MHA, and HNT-CS-MHA composite coatings on Ti alloy was carried out by FT-IR spectroscopy, and the result is shown in Figures 2(a)–2(d). Figure 2(a) shows a spectrum of the MHA coated on Ti alloy. The characteristic bands observed at 962 cm^{-1} symmetric stretching modes of P-O and 473 cm^{-1} doublet bending indicate the (ν1 and ν2) vibration modes of PO_4^{3-}, respectively. The absorption bands obtained at 1037(ν3b), 1092(ν3a) cm^{-1} and 566(ν4b, ac), 602(ν4a) cm^{-1} correspond to asymmetric (ν3) stretching modes and symmetric bending (ν4) modes of O-P-O ions, respectively. The bonds in the regions 635 cm^{-1} and 3570 cm^{-1} could be attributed to the presence of bending vibrational and stretching modes of the OH group in MHA. The characteristic peak assignments are in accordance with the literature data [29]. The characteristic IR bands observed for chitosan −3400 cm^{-1} for O-H stretching and 2940 cm^{-1} band for C-H stretch are as shown in Figure 2(b). The characteristic peaks of CS are at 1570 amide II (bending of the secondary amide group ($-NH_2$)) and 1123 (amine group), while the bands located at 1424 and 1373 cm^{-1} correspond to the C-H bonds on the CS chain [18, 19]. We could find that the characteristic band of MHA from the CS-MHA composite coating became less intense, and except for slight band shifts, these include the absence of O-H bending vibrational band at 635 cm^{-1}. On the contrary, the characteristic peaks of CS standing at 1643 amide I (C=O-NHR) disappeared, becoming less intense, which confirms the formation of possible electrostatic interaction and hydrogen bonding between the NH_3^+ of CS and PO_4^{3-} of HA [30].

The FT-IR spectra of HNT-MHA-coated implant surfaces are shown in Figure 2(c). The absorption band at 3492 cm^{-1} attributes to O-H stretching of water and that at 1652 cm^{-1} attributes to O-H deformation of water. The peaks at 667, 577, and 791 cm^{-1} are assigned for perpendicular Si-O stretching, and 1136 cm^{-1} is the stretch vibration absorption peak of Si-O, which corresponds to the broad O-H stretching signal at 3546 cm^{-1} [31]. The band observed at 526 cm^{-1} is deformation vibration of Al-O-Si. Some bonds are absent in the HNT-MHA composite coatings. These include deformation of Si-O-Si and O-H of inner hydroxyl groups which exhibited the peaks at 468 and 3621 cm^{-1}, respectively. Particularly, this indicates possible interactions between MHA and the surface functional groups of HNTs [32].

Figures 2(a)–2(c) peaks have similar peak positions as Figure 2(d) where the 1570 cm^{-1} vibration peak of N-H

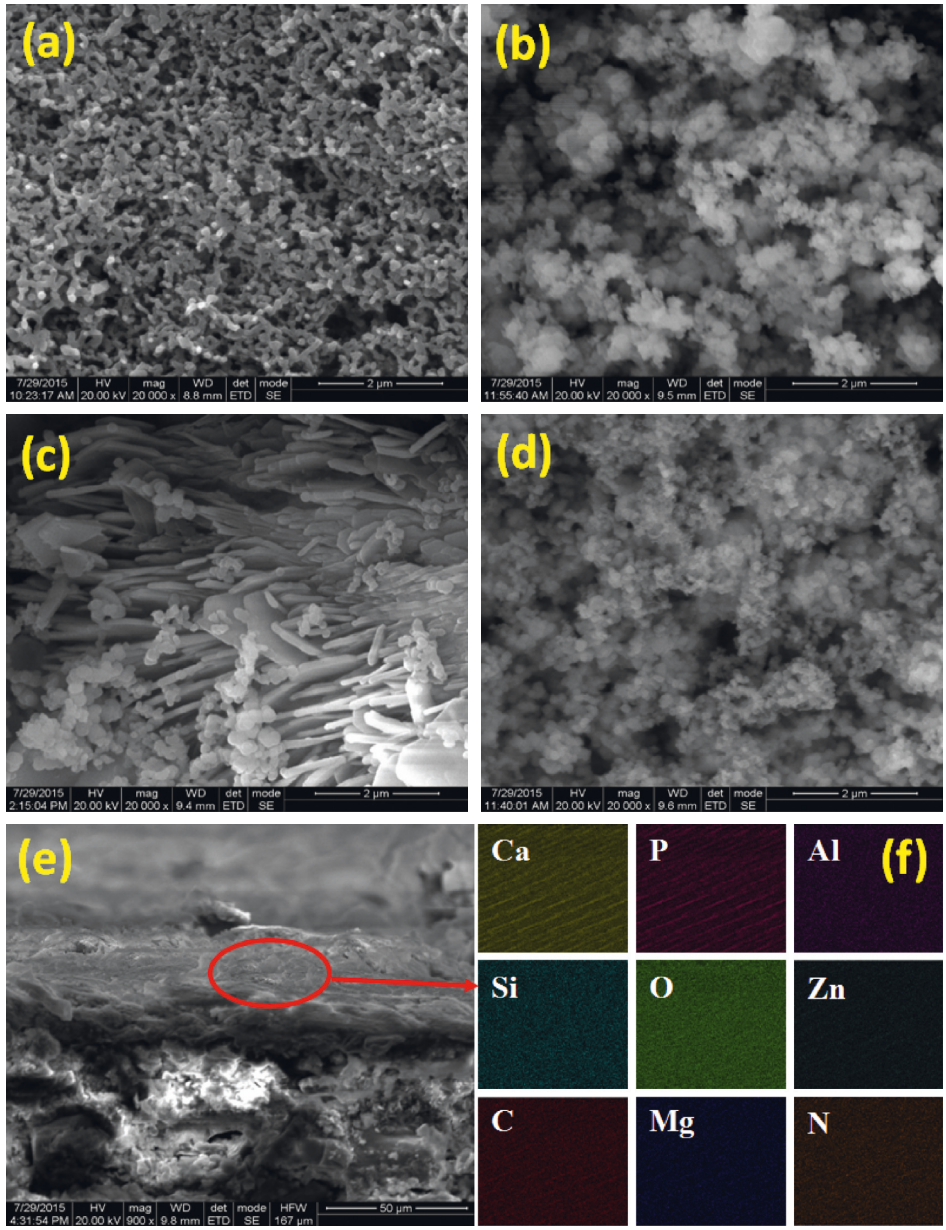

Figure 1: HR-SEM images of (a) MHA, (b) CS-MHA, (c) HNT-MHA, and (d) HNT-CS-MHA and (e) cross section and (f) elemental mapping images of HNT-CS-MHA composite coating on Ti6Al4V alloy surface.

shifted to 1578 cm^{-1} with less intensity, indicating the possible interaction between CS and HNT/MHA composites. The peaks at 1418 cm^{-1} originating from the symmetrical deformation modes of C-H groups in CS were also detected in the HNT-CS-MHA composite coatings. This strongly supports the formation of the HNT-CS-MHA composite coating on the Ti alloy sample.

3.3. XRD Analysis. The XRD patterns of the coated samples obtained in this work are shown in Figure 3. The XRD patterns of Figure 3(a) show the crystalline peaks by the main reflection at (2θ) 25.44°, 28.6°, 31.56°, 32.52°, and 42.32°, which confirms the formation of HA structure with matching those of the standard JCPDS No. 09–0432 data [33]. All of the diffraction peaks were sharp and well-resolved. The major intense peaks of Figure 3(b) were found at 2θ values of 20.66° corresponding to CS [34].

The remaining diffraction 2θ peaks were observed at MHA. The major intense peaks in Figure 3(c) were found at 2θ values of 12.2°, 20.74°, 24.3°, 35.32°, 37.7°, and 54.92° corresponding to HNT-MHA [35]. The XRD pattern of the as-received HNT showed peaks corresponding to JCPDS file No 29–1487 of HNT. No diffraction of unwanted peaks was found in the as-coated implant specimen, notably for the HNT-CS-MHAP composite (Figure 3(d)), and the diffraction peak positions shifted towards lower angles from the standard XRD patterns for HA. This is due to compression through interfacial bonding with the contracting polymeric matrix [36]. Bonding between MHAP, HNT, and CS occurs

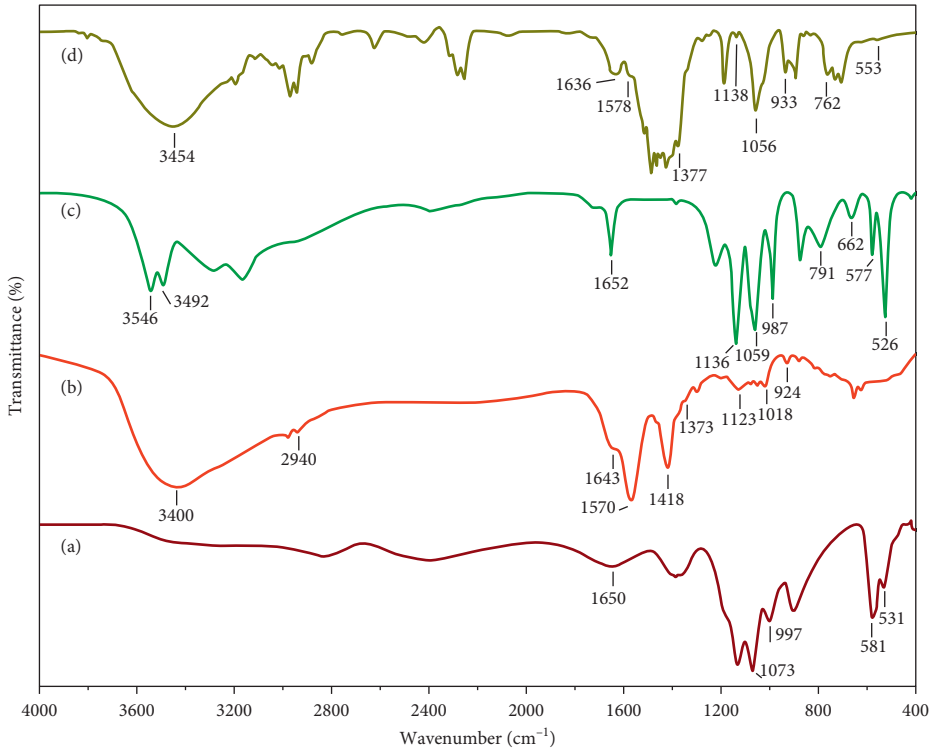

FIGURE 2: FT-IR spectra of (a) MHA coated on Ti6Al4V alloy, (b) CS-MHA coated on Ti6Al4V alloy, (c) HTN-MHA coated on Ti6Al4V alloy, and (d) HTN-CS-MHA composite coated on Ti6Al4V alloy.

through intermolecular hydrogen bonds and chelate interactions [37]. Thus, all these peaks demonstrate that the composite coating contains MHA, HNT, and CS crystalline phases.

3.4. Electrochemical Characterization. Polarization test was done in the range from −0.8 V to 0.2 V vs. SCE (Figure 4), at a scan rate of 1.0 mV s^{-1} in SBF solution after reaching a steady state potential value at 37°C. Polarization parameters (I_{corr} and E_{corr}) are given in Table 2. The corrosion potential (E_{corr}) and corrosion current density (I_{corr}) are given by the intersection of the Tafel lines' extrapolation. Corrosion is one of the most important problems for implant materials, and hence, the corrosion productions of this implant material gain are of importance [38]. Corrosion behaviors of the bare and coated implant substrates have been investigated by different methods such as polarization tests and EIS test. Figure 4 illustrates typical potentiodynamic polarization curves of uncoated and anodized Ti alloy substrates and MHA, CS-MHA, HNT-MHA, and HNT-CS-MHA coated specimen in SBF solution at room temperature. The mean values (standard deviation) of corrosion potential (E_{corr}) and corrosion current (I_{corr}) can be derived from the polarization curves and are summarized in Table 2. The corrosion potential (E_{corr}) of HNT-CS-MHA-coated specimen is −356 V, which is higher than that of the bare and anodized Ti6Al4V (-0.6168 and −0.592 V), MHA (−0.586), (CS-MHA (−0.561 V), and HNT-MHA (−0.438 V). In addition, the corresponding corrosion densities (I_{corr}) from Tafel fitting are 6.250×10^{-7}, 8.634×10^{-6}, 5.867×10^{-6}, 5.113×10^{-7}, 1.790×10^{-5}, and 9.140×10^{-6} for HNT-CS-MHA, MHA, CS-MHA, HNT-MHA, uncoated, and anodized Ti alloy, respectively. This shows that the HNT-CS-MHA coating significantly promotes corrosion resistance of the uncoated Ti alloy substrate in SBF. Generally, higher corrosion potential (E_{corr}) and lower corrosion current density (I_{corr}) indicate that the sample has a low corrosion rate and good corrosion resistance [39].

Since corrosion current density is proportional to the corrosion rate, lower corrosion current density also shows better corrosion resistance [40]. Therefore, we can conclude that the corrosion rate of HNT-CS-MHA is lower than those of MHA, CS-MHA, and HNT-MHA. This is due to its more dense surface coverage, as shown in Figure 1; thus, HNT-CS-MHA coating is more effective to prevent the contact between the electrolyte and the base metal material and then hinder the occurrence of corrosion reaction [41]. This result is also consistent with that in Table 2.

3.5. Electrochemical Impedance Spectroscopy Studies. The impedance results obtained from the Nyquist plots for the uncoated Ti alloy, anodized Ti alloy, MHA-Ti alloy, HNT-MHA-Ti alloy, CS-MHA-Ti alloy, and HNT-CS-MHA-Ti alloy in SBF solution under an open circuit potential (OCP) condition are shown in Figure 4(b). For the uncoated and anodized Ti alloy, the polarization resistance R_p value is observed as ($7.1542 \times 10^4\ \Omega\ cm^2$) and ($1.552 \times 10^5\ \Omega\ cm^2$), respectively. The R_p values for the MHA and CS-MHA-coated Ti6Al4V alloy are found to be greater ($3.373 \times 10^6\ \Omega\ cm^2$

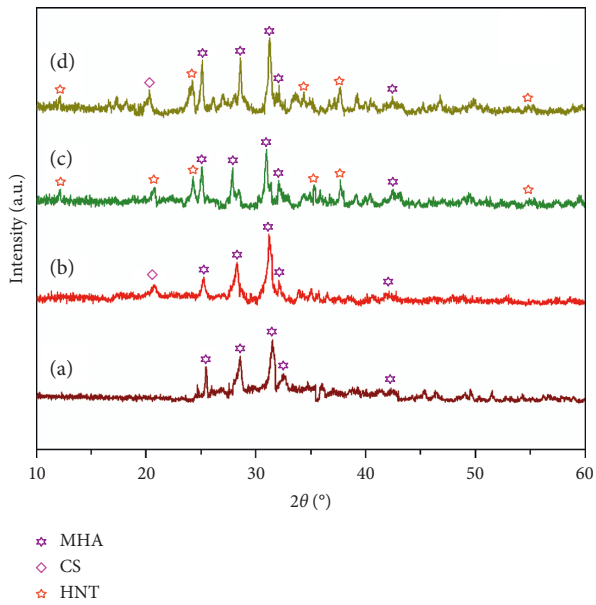

Figure 3: XRD patterns of (a) MHA coated on Ti6Al4V alloy, (b) CS-MHA coated on Ti6Al4V alloy, (c) HTN-MHA coated on Ti6Al4V alloy, and (d) HTN-CS-MHA composite coated on Ti6Al4V alloy.

and $4.023 \times 10^6\,\Omega\,cm^2$, respectively) than that of the anodized Ti alloy specimen. The HNT-MHA-coated Ti alloy shows a higher R_p value ($4.677 \times 10^6\,\Omega\,cm^2$) due to the effective protection of Ti by CS coating with an inactive coating underneath. The R_p value for the HNT-CS-MHA composite coating is found to be $5.644 \times 10^6\,\Omega\,cm^2$, which is still higher than that of the CS-MHA coated Ti alloy. The surface morphology, roughness, and thickness of the coating are the major factors affecting the corrosion resistance of titanium alloys in the SBF [42]. It is generally believed that if the density of the coating surface is higher, the corrosion resistance (R_p) of the surface is more [28, 43]. From these results, it is evident that the HNT-CS-MHA composite coating on Ti alloy is superior in terms of corrosion protection.

3.6. Adhesive Strength Analysis. The adhesive strength of the HNT-CS-MHA composite-coated Ti alloy (22.5 ± 1.3 MPa) was found to be greater than that of the HNT-MHA, CS-MHA, and MHA coatings, which were displayed as 20.1 ± 0.3, 16.2 ± 0.5, and 16.9 ± 1.7 MPa, respectively (Figure 5). Therefore, the data obviously revealed that the HNT-CS-MHA composite coatings possessed superior adhesion to the anodized Ti alloy surface. This adhesive strength of the HNT-CS-MHA composite coatings will make it suitable for orthodontics and orthopedic applications.

3.7. Antibacterial Activity Assay. Implantation infection leading to failure of orthopedic replacement is a major cause. So, the present study was aimed at developing a biomaterial with the incorporation of Zn and CS which possess intrinsic antibacterial activity [44]. Antibacterial effectiveness of HNT-CS-MHA composite-coated materials was investigated against the two prokaryotic strains such as *S. aureus* and *E. coli*, which are not only the typical representative of model Gram-positive and model Gram-negative bacteria, but also the most common bacteria in clinical infection, by the disc diffusion method, after incubation for 24 h at 37°C. The various zones of inhibition were found at different concentrations such as 20 μl, 40 μl, 65 μl, and 80 μl around the HNT-CS-MHA composite scraped sample against *S. aureus* and *E. coli* as shown in Figure 6 and Table 3.

As it can be seen from the antibacterial results, it is evident that the highest concentration of HNT-CS-MHA composite scraped sample exhibited excellent antibacterial activity against *S. aureus* and *E. coli.* When compared to the *S. aureus* bacteria, the HNT-CS-MHA composite-coated sample showed high antibacterial activity for *E. coli*, which exhibits that the composite scraped sample is more reactive against *E. coli.* For the HNT-CS-MHA composite, the measured inhibition zones for *E. coli* and *S. aureus* were increasing, and in particular, the coatings showed excellent activity against *E. coli*, which is due to the differences in the cell wall structure. The cell wall of the Gram-positive bacteria is composed of a thick layer of peptidoglycan, consisting of linear polysaccharide chains cross linked by short peptides, thus forming a more rigid structure leading to difficult penetration compared to the Gram-negative bacteria where the cell wall possesses a thinner layer of peptidoglycan [45]. Therefore, changes in the membrane structure of bacteria result in the increased antibacterial activity for the coatings against *E. coli.* From the results, it is well evident that the HNT-CS-MHA composite coating not only retards the bacterial adhesion but also effectively kills the adhered bacteria, suggesting effective and long-lasting antibacterial activity against both *E. coli* and *S. aureus*. Positively charged chitosan molecules might interact with negatively charged microbial cell membranes, leading to alterations in cell wall permeability and the leakage of intracellular compounds. This is a major reason for the destruction of bacteria [46]. Another plausible mechanistic pathway is that CS can chelate with trace metals, thereby hindering the enzyme activity of bacteria. The reason may be ascribed to the substitution of transition metal ion such as Zn^{2+} and CS in HA and also incorporation of HNTs plays a very important role in enhancing the activity, and hence, the surface area of the HNT-CS-MHA composite coating increases by forming bonds with the *S. aureus* and *E. coli* leading to cell death.

3.8. Cell Viability. The cell viability of MG63 cells on the HNT-CS-MHA composite-coated Ti alloy sample was carried out using the MTT assay, and the results are shown in Figure 7. The viability is calculated for the HNT-CS-MHA composite-coated Ti alloy sample with respect to control wells at 1, 4, and 7 days. The HNT-CS-MHA composite-coated Ti alloy sample exhibited considerable cell viability which is similar to that of the control group of the MG63 cells. The improved cell viability of the HNT-CS-MHA composite coating is mainly owing to the substitution of

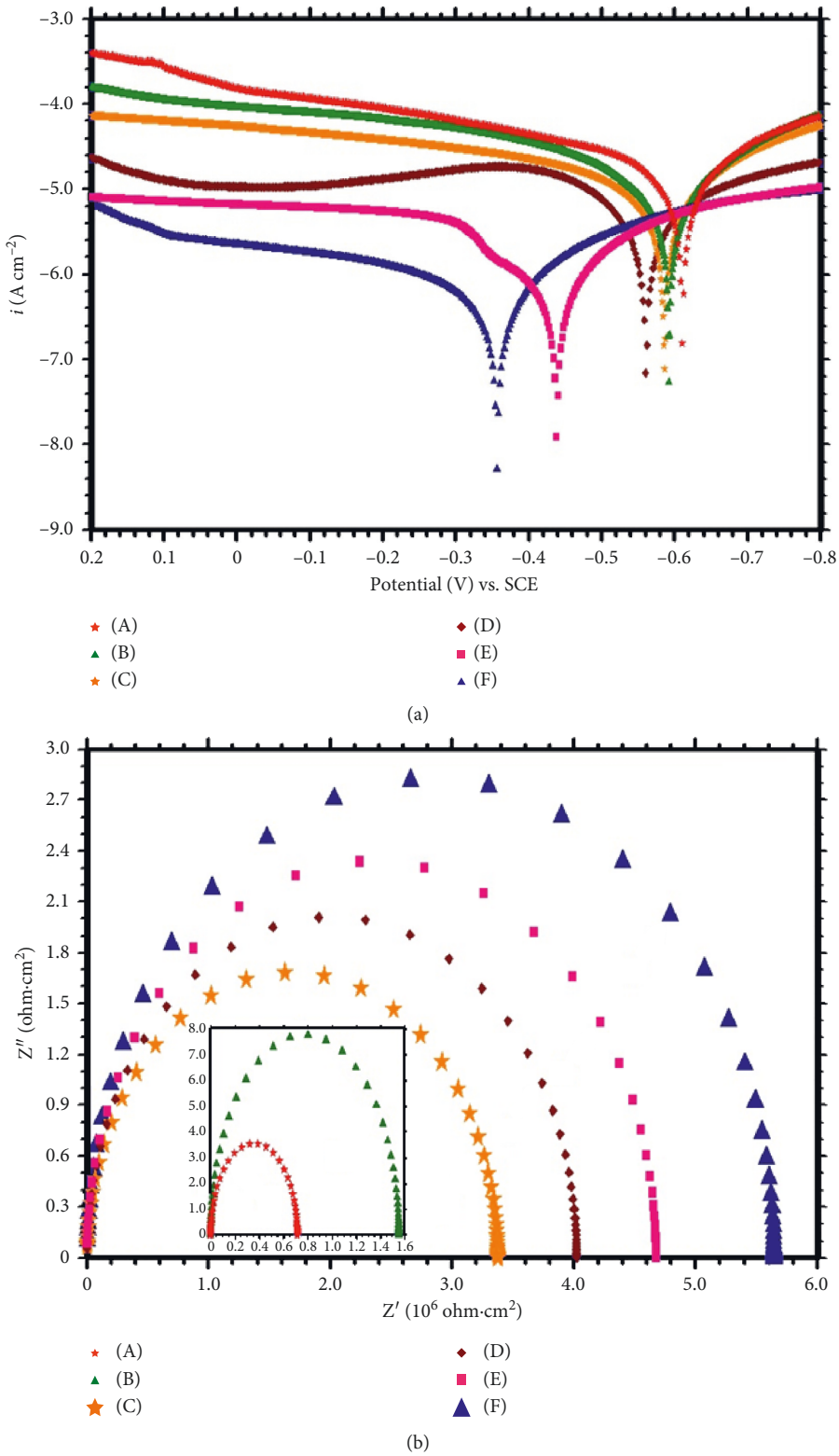

Figure 4: Potentiodynamic polarization (a) and Nyquist curves (b). (A) Uncoated Ti6Al4V alloy. (B) Anodized Ti6Al4V alloy. (C) MHA coated on Ti6Al4V alloy. (D) CS-MHA coated on Ti6Al4V alloy. (E) HTN-MHA coated on Ti6Al4V alloy. (F) HTN-CS-MHA composite coated on Ti6Al4V alloy in SBF solution.

minerals such as Mg^{2+} in HA and also Zn^{2+} incorporation in HNTs present in the HNT-CS-MHA composite coating [47, 48]. The cell viability of the HNT-CS-MHA composite coating is shown to enhance on increasing the days from 1 to 7 days of MG63 cell culture medium which indicates the nontoxic nature of this composite coating.

Table 2: Electrochemical parameters of uncoated and coated Ti6Al4V alloy.

Sample condition	E_{corr} (V vs. SCE)	I_{corr} ($\times 10^{-5}$ A cm^{-2})	R_p ($\times 10$)
Bare Ti6Al4V alloy	−0.6168	1.790×10^{-5}	7.1542×10^{4}
Anodized Ti6Al4V alloy	−0.592	9.140×10^{-006}	1.552×10^{5}
MHA/Ti6Al4V	−0.586	8.634×10^{-006}	3.373×10^{6}
CS-MHA/Ti6Al4V	−0.561	5.867×10^{-006}	4.023×10^{6}
HTN-MHA/Ti6Al4V	−0.430	6.113×10^{-007}	4.677×10^{6}
HTN-CS-MHA/Ti6Al4V	−0.356	6.250×10^{-007}	5.644×10^{6}

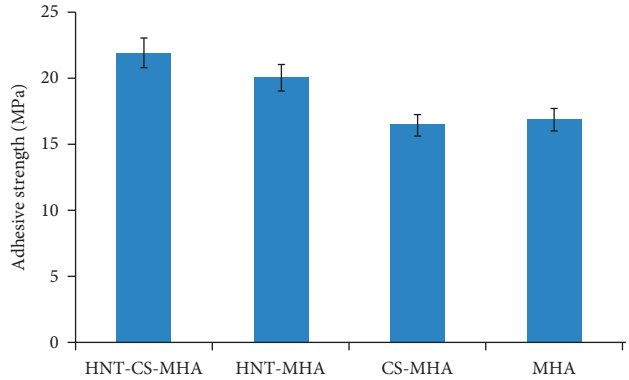

Figure 5: Adhesive strength of coated Ti6Al4V alloy.

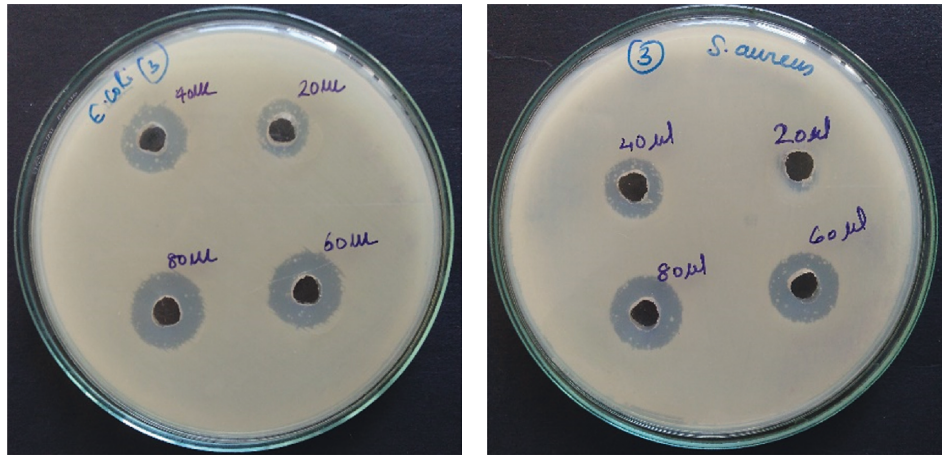

(a) (b)

Figure 6: Antibacterial activity of PEDOT-HNT-MHA composite coating against (a) *E. coli* and (b) *S. aureus*.

Table 3: Antibacterial activity assay.

Name of the bacteria	Zone of inhibition (mm)			
μl for sample	20 μl	40 μl	60 μl	80 μl
Escherichia coli	3	6	7.8	13
Staphylococcus aureus	1.1	3.4	5	9.7

All these cell viability results are in good agreement with the optical microscopic results. It can be seen from Figure 8(b) that a number of viable cells appeared in the HNT-CSMHA composite coating at 4 days of culture medium, and also the cell morphology was observed to be similar to the control group of MG63 cells. The HNT-CS-MHA composite coating at 7 days of culture medium (Figure 8(d)) indicates the presence of more number of viable cells confirming that the biocompatibility of the HNT-CS-MHA composite coating is not affected by the presence of HNT in the composite coating. From this result, it is furthermore evidenced that the presence of HNT as an ideal coating in the HNT-CS-MHA composite coating would impart excellent corrosion-resistive property to the composite coating without diminishing its bioactivity. As a result, the viability results evidently showed that the HNT-CS-MHA composite coating extensively increased the viability of cells (92.95%), which

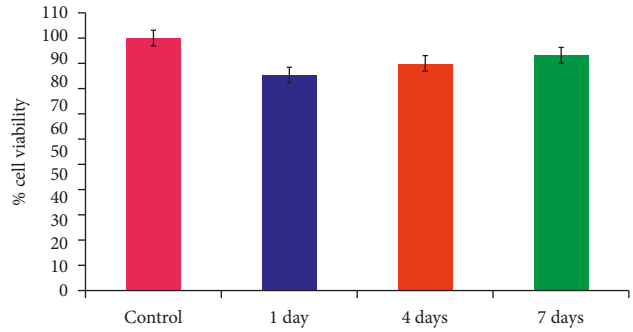

Figure 7: Bar diagram of HOS MG63 cells on HNT-CS-MHA composite coating for (a) control and (b) 1, (c) 4, and (d) 7 days of incubation.

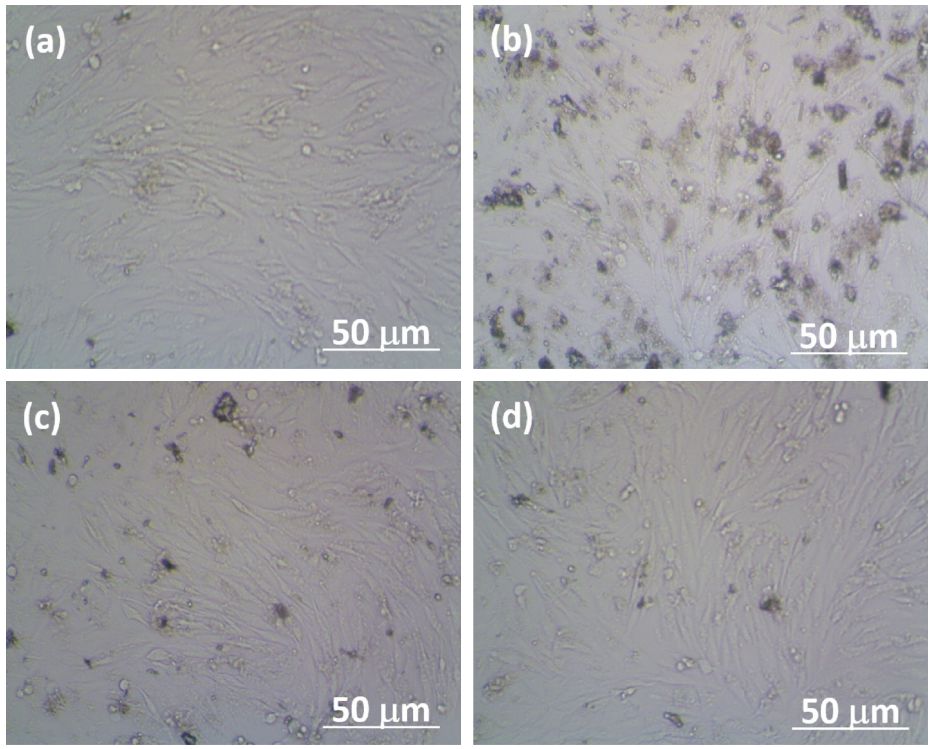

Figure 8: Optical images showing the viability of HOS MG63 cells on HNT-CS-MHA composite coating for (a) control and (b) 1, (c) 4, and (d) 7 days of incubation.

shows good biocompatibility and osteogenic induction ability.

4. Conclusion

Herein, we demonstrate the successful development of HNT-CS-MHA composite coating on Ti alloy by electrodeposition to improve the corrosion resistance and biological properties. The surface characterization using FT-IR and XRD spectra confirmed the formation of HNT-CS-MHA composite coating on Ti alloy. Electrochemical corrosion protection studies established that the HNT-CS-MHA composite coating on Ti alloy showed enhanced corrosion resistance which is ascribed to the HNT-CS-MHA coating on Ti6Al4V. The *in-vitro* antibacterial and cell viability studies of the HNT-CS-MHA composite coating on Ti6Al4V exhibited excellent antibacterial properties and bioactivity, respectively. Thus, the HNT-CS-MHA composite-coated Ti6Al4V will serve as an indispensable implant material with improved corrosion resistance and better bioactivity property for orthopedic applications.

Data Availability

The data used to support the findings of this study are available from the corresponding author upon request.

Conflicts of Interest

The authors declare that they have no conflicts of interest.

Acknowledgments

Rajavel acknowledges the major financial support from the Council of Scientific and Industrial Research (CSIR), New Delhi, India (01(2835)/15/EMR-II).

Supplementary Materials

The image shows the deposition of HNT-CS-MHA composite on Ti alloy surfaces. The coated implant could be used in biomedical applications. (*Supplementary Materials*)

References

[1] N. Peppas and R. Langer, "New challenges in biomaterials," *Science*, vol. 263, no. 5154, pp. 1715–1720, 1994.

[2] M. Jäger, C. Zilkens, K. Zanger, and R. Krauspe, "Significance of nano- and microtopography for cell-surface interactions in orthopaedic implants," *Journal of Biomedicine and Biotechnology*, vol. 2007, article 69036, 19 pages, 2007.

[3] A. Hunter, C. W. Archer, P. S. Walker, and G. W. Blunn, "Attachment and proliferation of osteoblasts and fibroblasts on biomaterials for orthopaedic use," *Biomaterials*, vol. 16, no. 4, pp. 287–295, 1995.

[4] R. Kumari and J. D. Majumdar, "Studies on corrosion resistance and bio-activity of plasma spray deposited hydroxylapatite (HA) based TiO 2 and ZrO 2 dispersed composite coatings on titanium alloy (Ti-6Al-4V) and the same after post spray heat treatment," *Applied Surface Science*, vol. 420, pp. 935–943, 2017.

[5] J. Ma, C. Z. Wang, C. L. Ban, C. Z. Chen, and H. M. Zhang, "Pulsed laser deposition of magnesium-containing bioactive glass film on porous Ti-6Al-4V substrate pretreated by micro-arc oxidation," *Vacuum*, vol. 125, pp. 48–55, 2016.

[6] A. Jemat, M. J. Ghazali, M. Razali, and Y. Otsuka, "Surface modifications and their effects on titanium dental implants," *BioMed Research International*, vol. 2015, p. 11, 2015.

[7] D. Wei, Q. Du, S. Guo et al., "Structures, bonding strength and in vitro bioactivity and cytotoxicity of electrochemically deposited bioactive nano-brushite coating/TiO 2 nanotubes composited films on titanium," *Surface and Coatings Technology*, vol. 340, pp. 93–102, 2018.

[8] H. Matsuno, A. Yokoyama, F. Watari, M. Uo, and Ta. Kawasaki, "Biocompatibility and osteogenesis of refractory metal implants, titanium, hafnium, niobium, tantalum and rhenium," *Biomaterials*, vol. 22, no. 11, pp. 1253–1262, 2001.

[9] E. Mohseni, E. Zalnezhad, and A. R. Bushroa, "Comparative investigation on the adhesion of hydroxyapatite coating on Ti-6Al-4V implant: a review paper," *International Journal of Adhesion and Adhesives*, vol. 48, pp. 238–257, 2014.

[10] M. Prakasam, J. Locs, K. Salma-Ancane, D. Loca, A. Largeteau, and L. Berzina-Cimdina, "Biodegradable materials and metallic implants-A review," *Journal of Functional Biomaterials*, vol. 8, no. 4, p. 44, 2017.

[11] Y. W. Song, D. Y. Shan, and E. H. Han, "Electrodeposition of hydroxyapatite coating on AZ91D magnesium alloy for biomaterial application," *Materials Letters*, vol. 62, no. 17-18, pp. 3276–3279, 2008.

[12] S. Durdu, K. Korkmaz, S. L. Aktuğ, and A. Ç.tuğ, "Characterization and bioactivity of hydroxyapatite-based coatings formed on steel by electro-spark deposition and micro-arc oxidation," *Surface and Coatings Technology*, vol. 326, pp. 111–120, 2017.

[13] Q. Yuan, J. Wu, C. Qin et al., "Spin-coating synthesis and characterization of Zn-doped hydroxyapatite/polylactic acid composite coatings," *Surface and Coatings Technology*, vol. 307, pp. 461–469, 2016.

[14] Q. Ding, X. Zhang, Y. Huang, Y. Yan, and X. Pang, "In vitro cytocompatibility and corrosion resistance of zinc-doped hydroxyapatite coatings on a titanium substrate," *Journal of Materials Science*, vol. 50, no. 1, pp. 189–202, 2014.

[15] Y. Huang, X. Zhang, H. Mao et al., "Osteoblastic cell responses and antibacterial efficacy of Cu/Zn co-substituted hydroxyapatite coatings on pure titanium using electrodeposition method," *RSC Advances*, vol. 5, no. 22, pp. 17076–17086, 2015.

[16] Y. Yan, Q. Ding, Y. Huang, S. Han, and X. Pang, "Magnesium substituted hydroxyapatite coating on titanium with nanotublar TiO2 intermediate layer via electrochemical deposition," *Applied Surface Science*, vol. 305, pp. 77–85, 2014.

[17] T. J. Webster, C. Ergun, R. H. Doremus, and R. Bizios, "Hydroxylapatite with substituted magnesium, zinc, cadmium, and yttrium. II. Mechanisms of osteoblast adhesion," *Journal of Biomedical Materials Research*, vol. 59, no. 2, pp. 312–317, 2001.

[18] A. Molaei, M. Yari, and M. R. Afshar, "Investigation of halloysite nanotube content on electrophoretic deposition (EPD) of chitosan-bioglass-hydroxyapatite-halloysite nanotube nanocomposites films in surface engineering," *Applied Clay Science*, vol. 135, pp. 75–81, 2017.

[19] H. A. Afshar and A. Ghaee, "Preparation of aminated chitosan/alginate scaffold containing halloysite nanotubes with improved cell attachment," *Carbohydrate Polymers*, vol. 151, pp. 1120–1131, 2016.

[20] M. Liu, R. He, J. Yang, W. Zhao, and C. Zhou, "Stripe-like clay nanotubes patterns in glass capillary tubes for capture of tumor cells," *ACS Applied Materials and Interfaces*, vol. 8, no. 12, pp. 7709–7719, 2016.

[21] N. S. Radda, W. H. Goldmann, R. Detsch et al., "Electrophoretic deposition of tetracycline hydrochloride loaded halloysite nanotubes chitosan/bioactive glass composite coatings for orthopedic implants," *Surface and Coatings Technology*, vol. 327, pp. 146–157, 2017.

[22] P. Karthikeyan, L. Mitu, K. Pandian, G. Anbarasu, and R. Rajavel, "Electrochemical deposition of a Zn-HNT/p(EDOT-co-EDOP) nanocomposite on LN SS for antibacterial and anti-corrosive applications," *New Journal of Chemistry*, vol. 41, no. 12, pp. 4758–4762, 2017.

[23] Q. Sheng, D. Zhang, Q. Wu, J. Zheng, and H. Tang, "Electrodeposition of prussian blue nanoparticles on polyaniline coated halloysite nanotubes for nonenzymatic hydrogen peroxide sensing," *Analytical Methods*, vol. 7, pp. 6896–6903, 2015.

[24] S. Ranganatha and T. V. Venkatesha, "Fabrication and electrochemical characterization of Zn-halloysite nanotubes composite coatings," *RSC Advances*, vol. 4, pp. 31230–31238, 2014.

[25] C. Chao, B. Zhang, R. Zhai, X. Xiang, J. Liu, and R. Chen, "Natural nanotube-based biomimetic porous microspheres for significantly enhanced biomolecule immobilization," *ACS Sustainable Chemistry and Engineering*, vol. 2, no. 3, pp. 396–403, 2013.

[26] P. Karthikeyan, S. Sathishkumar, K. Pandian, L. Mitu, and R. Rajavel, "Novel copper doped Halloysite Nano Tube/silver-poly(pyrrole-co-3,4-ethylenedioxythiophene) dual layer coatings on low nickel stainless steel for anti-corrosion applications," *Journal of Science: Advanced Materials and Devices*, vol. 3, no. 1, pp. 59–67, 2018.

[27] T. Kokubo and H. Takadama, "How useful is SBF in predicting in vivo bone bioactivity?," *Biomaterials*, vol. 27, no. 15, pp. 2907–2915, 2006.

[28] G. Singh, H. Singh, and B. S. Sidhu, "In vitro corrosion investigations of plasma-sprayed hydroxyapatite and hydroxyapatite-calcium phosphate coatings on 316L SS," *Bulletin of Materials Science*, vol. 37, no. 6, pp. 1519–1528, 2014.

[29] M. Manoj, D. Mangalaraj, N. Ponpandian, and C. Viswanathan, "Core-shell hydroxyapatite/Mg nanostructures: surfactant free facile synthesis, characterization and their in vitro cell viability studies against leukaemia cancer cells (K562)," *RSC Advances*, vol. 5, no. 60, pp. 48705–48711, 2015.

[30] T. A. Salah, A. M. Mohammad, M. A. Hassan, and B. E. El-Anadouli, "Development of nano-hydroxyapatite/chitosan composite for cadmium ions removal in wastewater treatment," *Journal of the Taiwan Institute of Chemical Engineers*, vol. 45, no. 4, pp. 1571–1577, 2014.

[31] H. Lun, J. Ouyang, and H. Yang, "Natural halloysite nanotubes modified as an aspirin carrier," *RSC Advances*, vol. 4, pp. 44197–44202, 2014.

[32] L. Fan, J. Zhang, and A. Wang, "In situ generation of sodium alginate/hydroxyapatite/halloysite nanotubes nanocomposite hydrogel beads as drug-controlled release matrices," *Journal of Materials Chemistry B*, vol. 1, no. 45, pp. 6261–6270, 2013.

[33] S. Yang, H. He, L. Wang, X. Jia, and H. Feng, "Oriented crystallization of hydroxyapatite by the biomimetic amelogenin nanospheres from self-assemblies of amphiphilic dendrons," *Chemical Communications*, vol. 47, no. 36, pp. 10100–10102, 2011.

[34] S. Kumar and J. Koh, "Physiochemical, Physiochemical, optical and biological activity of chitosan-chromone derivative for biomedical applications," *International Journal of Molecular Sciences*, vol. 13, no. 5, pp. 6102–6116, 2012.

[35] M. Chozhanathmisra, D. Govindaraj, P. Karthikeyan, and R. Rajavel, "Antibacterial efficacy of halloysite nanotube minerals substituted hydroxyapatite composite on titanium alloy using electrodeposition method," *Asian Journal of Chemistry*, vol. 30, no. 10, pp. 2264–2268, 2018.

[36] M. R. Nikpour, S. M. Rabiee, and M. Jahanshahi, "Synthesis and characterization of hydroxyapatite/chitosan nanocomposite materials for medical engineering applications," *Composites Part B: Engineering*, vol. 43, no. 4, pp. 1881–1886, 2012.

[37] C. Zhang and T. Liu, "A review on hybridization modification of graphene and its polymer nanocomposites," *Chinese Science Bulletin*, vol. 57, no. 23, pp. 3010–3021, 2012.

[38] G. Manivasagam, D. Dhinasekaran, and A. Rajamanickam, "Biomedical implants: corrosion and its prevention-a review," *Recent Patents on Corrosion Science*, vol. 2, no. 1, pp. 40–54, 2010.

[39] H. Liu, Y. X. Leng, G. Wan, and N. Huang, "Corrosion susceptibility investigation of Ti-O film modified cobalt-chromium alloy (L-605) vascular stents by cyclic potentiodynamic polarization measurement," *Surface and Coatings Technology*, vol. 206, no. 5, pp. 893–896, 2011.

[40] J. Liu, Y. Lou, C. Zhang et al., "Improved corrosion resistance and antibacterial properties of composite arch-wires by N-doped TiO2 coating," *RSC Advances*, vol. 7, no. 69, pp. 43938–43949, 2017.

[41] A. Ganash, "Effect of current density on the corrosion protection of poly(otoluidine)-coated stainless steel," *International Journal of Electrochemical Science*, vol. 9, pp. 4000–4013, 2014.

[42] R. Zhang, X. Ai, Y. Wan, Z. Liu, D. Zhang, and S. Feng, "Surface corrosion resistance in turning of titanium alloy," *International Journal of Corrosion*, vol. 2015, pp. 1–8, 2015.

[43] E. C. Meng, S. K. Guan, H. X. Wang et al., "Effect of electrodeposition modes on surface characteristics and corrosion properties of fluorine-doped hydroxyapatite coatings on Mg-Zn-Ca alloy," *Applied Surface Science*, vol. 257, no. 11, pp. 4811–4816, 2011.

[44] X. Zhai, C. Sun, K. Li et al., "Synthesis and characterization of chitosan-zinc composite electrodeposits with enhanced antibacterial properties," *RSC Advances*, vol. 6, no. 52, pp. 46081–46088, 2016.

[45] W. W. Navarre and O. Schneewind, "Surface proteins of gram-positive bacteria and mechanisms of their targeting to the cell wall envelope," *Microbiology and Molecular Biology Reviews*, vol. 63, no. 1, pp. 174–229, 1999.

[46] C. Ning, L. Zhou, Y. Zhu et al., "Influence of surrounding cations on the surface degradation of magnesium alloy implants under a compressive pressure," *Langmuir*, vol. 31, no. 50, pp. 13561–13570, 2015.

[47] Q. H. Bao, C. Sun, C. Zhang, and J. Q. Zhang, "Dip coated magnesium-substituted hydroxyapatite coatings on magnesium alloy for biomedical applications," *Journal of Biomimetics, Biomaterials and Biomedical Engineering*, vol. 25, pp. 83–89, 2015.

[48] E. S. Thian, T. Konishi, Y. Kawanobe et al., "Zinc-substituted hydroxyapatite: a biomaterial with enhanced bioactivity and antibacterial properties," *Journal of Materials Science: Materials in Medicine*, vol. 24, no. 2, pp. 437–445, 2012.